Numerical simulations of the geospace response to the arrival of a perfect interplanetary coronal mass ejection

Daniel T. Welling [1], Jeffrey J. Love [2], E. Joshua Rigler [2], Denny M. Oliveira [3,4], Colin M. Komar [5,4]

[1]University of Texas at Arlington Department of Physics, Arlington, Texas, United States
[2]Geomagnetism Program, Geologic Hazards Science Center, U.S. Geological Survey, Denver, Colorado, United States
[3]Goddard Planetary Heliophysics Institute, University of Maryland, Baltimore County, Baltimore, MD, USA
[4]NASA Goddard Space Flight Center, Greenbelt, MD, USA
[5]The Catholic University of America, Washington DC, USA

Key Points:

- A "perfect" ICME arrival at Earth is simulated using the Space Weather Modeling Framework.
- Predicted surface dB/dt surpasses 300 nT/s regionally, exceeding previous estimations of such an event.
- Simulated response surpasses that of real world extreme events, advancing our understanding of a space weather worst-case scenario.

Corresponding author: Daniel Welling, dwelling@uta.edu

Abstract

Understanding extreme space weather events in terms of the geospace response is a critical step towards protecting vulnerable technological infrastructure. This is particularly relevant for the effects of geomagnetically induced currents (GICs) on ground-based power grids, which can be approximated by examining the rate of change of the surface magnetic field, dB/dt. In a previous study, Tsurutani and Lakhina (2014) created estimates for a perfect, isolated interplanetary coronal mass ejection (ICME) and performed a simple calculation for the response of geospace, including dB/dt. In this study, the estimates of Tsurutani and Lakhina (2014) are used to drive a coupled magnetohydrodynamic (MHD)-ring current-ionosphere model of geospace to obtain more detailed and physically accurate estimates of the geospace response to such an ICME. The sudden impulse phase is examined; calculations of surface dB/dt, Dst index, and day side magnetopause compression are compared to the less sophisticated estimations of Tsurutani and Lakhina (2014). It is found that while the previous study yielded similar estimates for Dst rise and magnetopause compression, dB/dt estimates are as much as an order of magnitude lower than the results obtained via physics-based modeling. This work shows that dB/dt values in excess of $30nT/s$ are found as low as 40° magnetic latitude. It is also shown that the direction of the interplanetary magnetic field plays a critical role: under southward IMF conditions, magnetopause erosion combines with strong region 1 Birkeland currents to intensify the dB/dt response. The values obtained here surpass those found in real-world events and sets the bar for the upper threshold of extreme GIC activity at Earth.

1 Introduction

With the arrival, at Earth, of the shock wave of an interplanetary coronal mass ejection (ICME), a geomagnetic sudden impulse (SI) is generated in ground-level magnetometer data (Araki, 1977; Joselyn & Tsurutani, 1990), prominently seen in the horizontal component data acquired at low and mid-latitude ground-based observatories. Magnetic storms often commence with such an impulse, and the most intense magnetic storms always commence with an impulse (e.g., Gonzalez, Echer, Tsurutani, De Gonzalez, & Dal Lago, 2011). The future occurrence of rare magnetic superstorms could have widespread deleterious impacts on modern technological systems (Cannon et al., 2013; National Research Committee on the Societal and Economic Impacts of Severe Space Weather Events, 2008). In this context, the Carrington event of 1859 has taken on particular significance – it is, by some estimates, the most intense magnetic storm ever directly measured (Lakhina, Alex, Tsurutani, & Gonzalez, 2012; Tsurutani, 2003). Fundamental research into the physical nature of extreme space-weather events has included data-driven, numerical simulation of a Carrington-class ICME (Manchester, Ridley, Gombosi, & DeZeeuw, 2006), ICME-driven sudden commencement action on the magnetosphere-ionosphere system (A. Ridley, De Zeeuw, Manchester, & Hansen, 2006), and simulation of the resulting storm main-phase (e.g., Li, Temerin, Tsurutani, & Alex, 2006; Ngwira, Pulkkinen, Kuznetsova, & Glocer, 2014).

Recently, Tsurutani and Lakhina (2014) have estimated, on the basis of qualitative physical arguments, solar-wind parameters at 1 astronomical unit for a theoretically most-extreme ICME. They refer to these as the conditions of a "perfect" ICME. They infer that these perfect conditions would generate a giant sudden impulse and a magnetic storm having an intensity far exceeding anything ever measured. They suggest, furthermore, that the hazards of such a hypothetical event, especially hazards to electric-power grids posed by the induction of geoelectric fields in the conducting solid Earth, should be further studied. Motivated by the work of Tsurutani and Lakhina (2014), we use their estimates of the perfect ICME to drive a numerical simulation of the response of the coupled ionosphere-magnetosphere system to the sudden impulse during the ICME's arrival. Results inform projects concerned with the assessment and mitigation of space-

weather related hazards and risks (Eastwood et al., 2017), such as the National Science and Technology Council (2015) and allied international organizations (e.g., Schrijver, 2015).

2 Perfect Solar Wind Conditions

The solar wind conditions preceding and during the hypothetical perfect sudden commencement event are adapted from Tsurutani and Lakhina (2014). For the first six hours, an ambient solar wind velocity of 350 km/s and density of 5 cm^{-3} are used. The IMF during this period is oriented purely southward with a magnitude of -5 nT. At 2:00 UT, the IMF turns northward for a period of two hours before returning southward. This sets up more realistic magnetospheric conditions in the numerical simulation. At 6:00 UT, the conditions impulsively change following the analysis of Tsurutani and Lakhina (2014). The velocity jumps to 2700 km/s. This assumes a near-Sun ICME speed of 3000 km/s that is only slowed 10% by an inner heliosphere that has been recently "cleaned out" by a recent preceding ICME. The ICME density jumps to 20 cm^{-3} using a shock jump ratio of 4. The IMF magnitude changes to 127 nT based on the empirical relationship from Gonzalez et al. (1998). Two separate orientations are considered here: a northward IMF case and a southward IMF case. A purely frontal shock is assumed as these shocks can result in stronger geomagnetic activity (Oliveira et al., 2018; Oliveira & Raeder, 2014, 2015), whereas small impact angles are correlated with faster sudden impulse responses (e.g., Guo, Hu, & Wang, 2005; Wang, Li, Huang, & Richardson, 2006). The net result is input conditions for a hypothetically perfect single sudden commencement event. A summary plot of the solar conditions can be found in the supplementary material; time series data is available in the repository listed in the acknowledgments.

3 Modeling Method

The interaction of these solar wind drivers with the Earth's magnetosphere and ionosphere are simulated using the Space Weather Modeling Framework (SWMF) (Tóth et al., 2005, 2012). The SWMF executes, synchronizes, and couples different models of the space environment to obtain a complete description of magnetosphere-ionosphere dynamics. For this simulation, three models are employed. The first is the Block Adaptive Tree Solar wind Roe-type Upwind Scheme (BATS-R-US) code, a flexible, finite-volume magnetohydrodynamic (MHD) model (D. De Zeeuw, Gombosi, Groth, Powell, & Stout, 2000; Groth, De Zeeuw, Gombosi, & Powell, 2000; Powell, Roe, & Linde, 1999). BATS-R-US has a long history of terrestrial magnetosphere simulations (e.g., Ilie, Liemohn, & Ridley, 2010; Song, DeZeeuw, Gombosi, Groth, & Powell, 1999; D. T. Welling & Zaharia, 2012; Zhang et al., 2007) including simulations of extreme driving (Ngwira et al., 2014, 2013; A. Ridley et al., 2006). Via the SWMF, it is coupled to a height-integrated ionospheric electrodynamics model (A. J. Ridley, De Zeeuw, Gombosi, & Powell, 2001), which calculates the ionospheric electric potential and horizontal currents from the MHD Birkeland currents. The electric potential is returned to BATS-R-US to set the convection electric field. To better capture ring current dynamics, the Rice Convection Model (RCM) (Harel et al., 1981; Sazykin & Stanislav, 2000; Toffoletto, Sazykin, Spiro, & Wolf, 2003) is also employed. It receives plasma sheet conditions, magnetic and electric fields from the other models and returns plasma pressure and number density to BATS-R-US (D. L. De Zeeuw et al., 2004). Using this and similar model combinations, the SWMF has demonstrated skill in reproducing magnetospheric dynamics (Rastätter et al., 2011; A. J. Ridley et al., 2002; D. T. Welling et al., 2015; D. T. Welling & Ridley, 2010), Birkeland current distributions (Korth, Rastätter, Anderson, & Ridley, 2011), ground magnetic perturbations (Yu & Ridley, 2008, 2009b), surface dB/dt (Pulkkinen et al., 2013), and associated geomagnetic indices (Glocer, 2016; Haiducek, Welling, Ganushkina, Morley, & Ozturk, 2017; Rastätter et al., 2013).

The exact configuration of these models follows Pulkkinen et al. (2013) with some notable exceptions:

1. The inner boundary is set at 1.75 R_E instead of 2.5 R_E. This prevents situations where the magnetopause touches the inner boundary under extreme driving.
2. The grid resolution follows Figure 1 of D. T. Welling and Ridley (2010). Near the inner boundary, cell sizes are cubes of 1/8 R_E width. The inner magnetosphere and magnetopause during the SI lie within regions of 1/4 R_E cell size.
3. All models are coupled at a frequency of 1 Hz, as opposed to typical values of .1Hz. This ensures the models stay synchronized during the rapid SI.
4. To simplify analysis, the dipole tilt is set to zero, i.e., the magnetic dipole is aligned with the rotation axis.

Input files are available in the repository listed in the acknowledgments. Using this setup, two simulations are performed: a purely northward IMF sudden commencement and a purely southward IMF case.

Ground magnetic perturbations are calculated using chains of *virtual magnetometers* (Yu & Ridley, 2009b). These are probes of the coupled-model system that perform Biot-Savart integrals of four distinct current systems:

1. All currents within the MHD domain,
2. Birkeland currents in the "gap region" between the MHD inner boundary and the ionosphere, mapped along assumed dipole field lines,
3. Ionospheric Hall currents,
4. Ionospheric Pedersen currents.

The four contributions are used to calculate the total perturbation in three orthogonal directions; only the two horizontal components (north-south, "X" and east-west, "Y") are examined here. Because the geomagnetic axis is set to be parallel with the Earth's rotational axis in this simulation, geomagnetic and geographic directions are equivalent. Virtual magnetometer results have 1 Hz resolution. The efficacy of these tools in reproducing observations and their role in space weather forecasting has recently been reviewed by D. Welling (2019).

4 Simulation Results

Figure 1 shows the response of the magnetosphere-ionosphere system to the hypothetical perfect ICME arrival, for both the northward and southward cases. The top row of Figure 1 (frames a-d) illustrates the moment when the ICME shock wave arrives at the bow shock (approximately 6:00:40 simulation time, herein referred to as $T_{Arrival}$). At this point, the northward IMF case (frames a, b) is the same as the southward case (frames c,d). 40 seconds later (second row, frames e through i), the ICME has begun to compress the magnetosphere. In agreement with previous studies of sudden impulses in global MHD models (Kataoka, Fukunishi, Fujita, Tanaka, & Itonaga, 2004; Slinker et al., 1999; Yu & Ridley, 2009a), low latitude flow vortices form along the day side magnetopause and propagate with the shock to the night side (not shown). These drive Birkeland currents connecting to the day side ionosphere (frames f and g), propagating to the night side with the associated magnetospheric flow vortices. At $T_{Arrival} + 1:10$ (Figure 1, third row), the two cases begin to diverge. The southward oriented IMF begins to erode the day side magnetopause rapidly (frame l), driving the magnetopause further inwards compared to the northward IMF case (frame i). While the spatial distribution of the Birkeland currents are similar between the two cases, the additional contribution from reconnection-driven Birkeland currents creates stronger magnitudes in the southward IMF case (3.3 μ/Am^2 peak, frame k) as compared to the northward case (frame

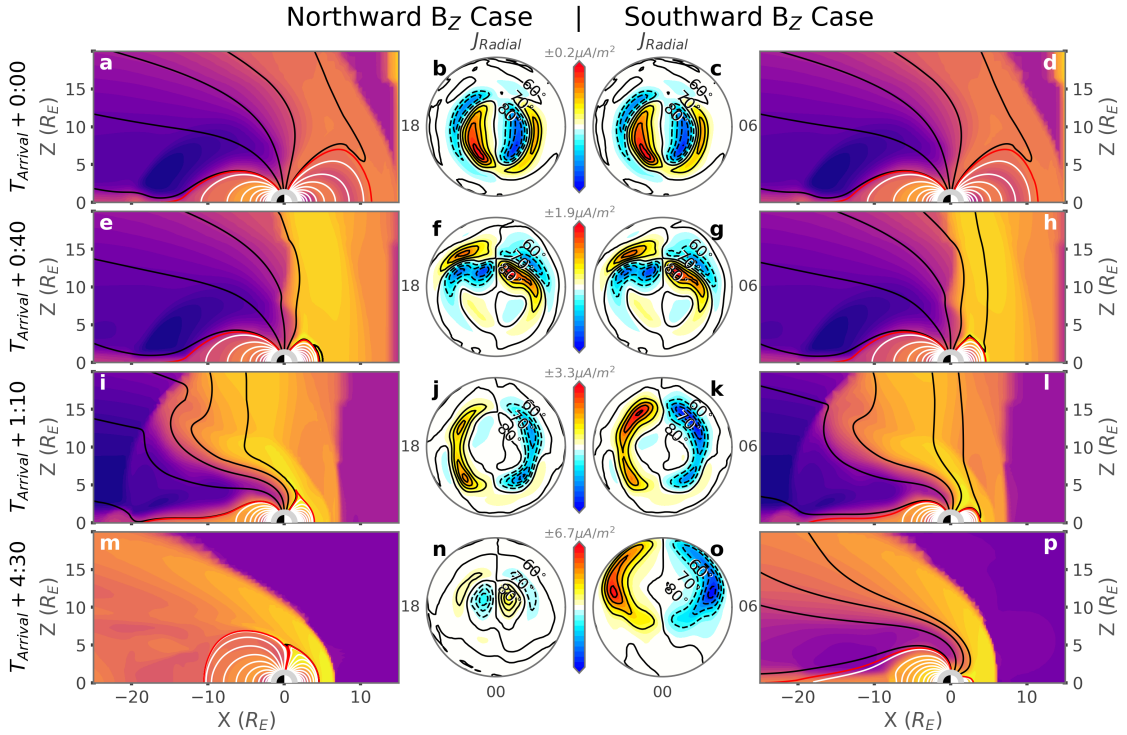

Figure 1. Each row shows results from a different point in the simulation. Results for the northward IMF case are shown in the leftmost two columns, results for the southward case on the right. The leftmost and rightmost columns show the state of the magnetosphere in the noon-midnight meridian plane in terms of magnetic field (black lines for open field, white lines for closed field, and red lines for the last-closed line) and plasma thermal pressure (colored contours). The polar plots illustrate the Birkeland currents flowing into (blue) and out of (yellow) the northern hemisphere. The scale of the current contours is shown via the color bar at the center of the figure.

j). After passage of the ICME ($T_{Arrival}$+4 : 30, bottom row), the two simulations have relaxed into a new pseudo-steady state. Dynamics are well characterized by forward and reverse magnetospheric convection; typical Birkeland current patterns for the southward and northward case, respectively. Again, reconnection has eroded the magnetopause further inward in the southward case (frame p) than in the northward case (frame m), where compression acts alone. Noteworthy for the southward case (frame o) is the extreme Birkeland current amplitudes (6.7 μAm^2) and their low latitudes on the day side due to from magnetopause erosion.

The simulated D_{ST} values illustrate the impact of the perfect ICME arrival. Figure 2(a) shows D_{ST} from the northward IMF and southward IMF cases. Values are plotted against time relative to $T_{Arrival}$. For the northward case, D_{ST} reaches a peak of 234.0 nT, slightly lower than the (Tsurutani & Lakhina, 2014) estimate of 245 nT. For the southward case, the peak D_{ST} is of larger magnitude (268.7 nT) and is reached slightly sooner than the northward IMF case. Despite small differences between the northward and southward cases, both are congruent with the estimates of (Tsurutani & Lakhina, 2014).

Before the simulated ICME makes contact with the bow shock ($T < T_{Arrival}$), a precursor signature is observed in D_{ST}. These signatures arise from the intense cur-

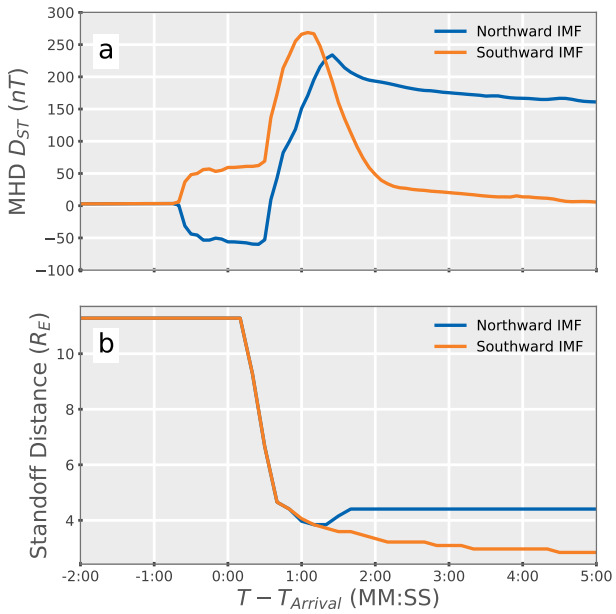

Figure 2. Summary of the northward IMF (blue) and southward IMF (orange) simulated sudden impulse in terms of the D_{ST} index (frame a) and the magnetopause stand-off distance (frame b).

rent sheet that forms at the IMF discontinuity as it jumps from $-5\ nT$ to $\pm 127\ nT$. Because the virtual D_{ST} is the result of a Biot-Savart integral covering the entire MHD domain, the ICME current sheet begins to drive pre-arrival signatures as soon as it enters the MHD model's upstream boundary at $+32\ R_E$. Immediately before impulse onset, the precursor signature reaches $\sim \pm 50\ nT$, growing slightly as the shock approaches Earth, with the orientation corresponding to the direction of the IMF. The addition of the precursor signal to the sudden impulse signal can explain the differences in magnitude and timing between the northward and southward IMF cases. This signal is a result of the magnetostatic assumption implicit in the Biot-Savart integral. Under the more realistic MHD formalism, such a magnetic signal propagates with local plasma wave speeds and could not arrive faster than the shock, as the relevant upstream Mach numbers are all greater than 1.

Figure 2(b) shows the magnetopause stand-off distance for both the northward and southward IMF cases. The values are calculated by identifying the first computational cell in the MHD domain whose field line is open to the solar wind when progressing radially from the Sun to the Earth. Though the magnetopause is pushed very close to the inner boundary, several grid cells separate the two. The ICME leads to extreme compression of the day side magnetosphere. For the northward IMF case, the stand-off distance reaches a new equilibrium at 4.41 R_E, reasonably agreeing with the estimate from Tsurutani and Lakhina (2014). For the southward case, day side reconnection further erodes the magnetopause to a stand-off distance of 2.84 R_E. The polarity of the IMF is clearly an important factor in setting the stand-off distance.

Figure 3 shows the effect of the ICME on the surface magnetic field in the geomagnetic north-south direction for a latitudinal chain of magnetometers all located at local noon. Both the magnetic perturbation (ΔB_N, frames a and c) as well as the time derivative (dB_N/dt, frames b and d) are shown. The geomagnetic east-west component results (not shown) are drastically weaker than the north-south component, except at auroral

latitudes where the values are of the same order as the north-south component. The figure covers seven minutes of the event.

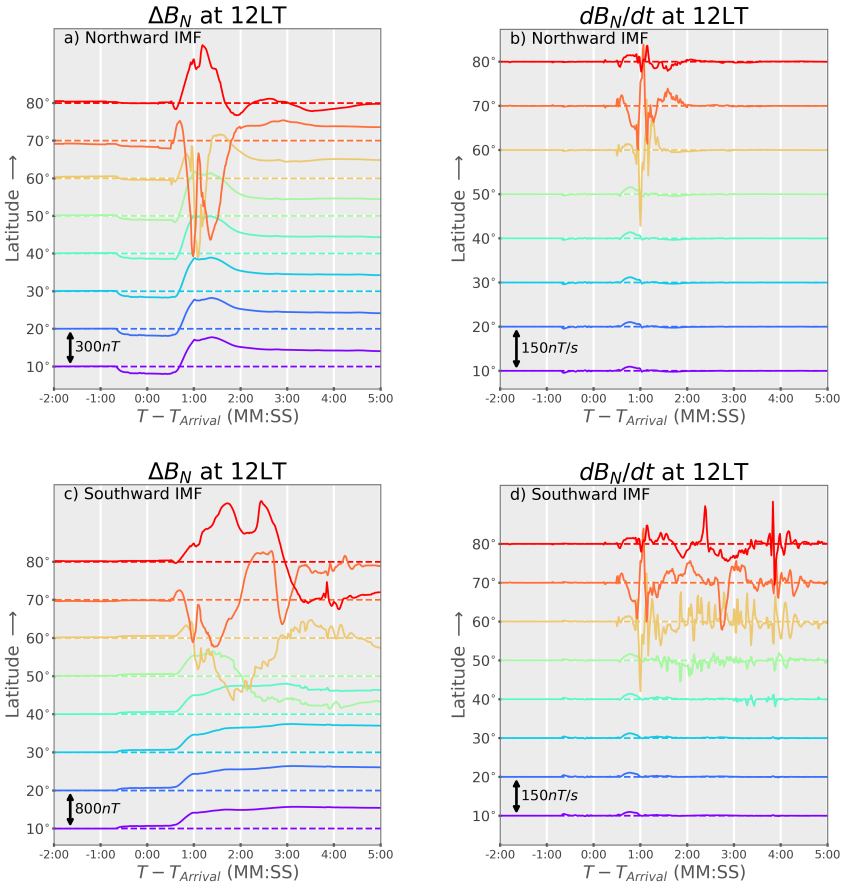

Figure 3. Virtual magnetometer surface perturbation results in the magnetic north-south direction for stations situated at local noon, two minutes before shock arrival through five minutes afterwards. Both ΔB_N (left column) and dB_N/dt (right column) are shown. Top row (frames a-b) shows results for the northward IMF case; bottom row (frames c-d) shows the results for the southward case. Stations are arranged in latitudinal order with the lowest latitudes on the bottom. For each curve, the dashed line of the same color shows where $\Delta B_N = 0$ or $dB_N/dt = 0$. The black arrow in the lower-left of each frame shows the scale of the perturbations.

Starting with the northward case (Figure 3, frames a-b), it can be seen that the impulse onset organizes itself into three distinct phases. The first phase is the precursor phase, where the current sheet within the IMF discontinuity is driving the precursor signal at all latitudes and local times. The strength of the disturbance grows to $-50\ nT$ at middle latitudes. The second phase, beginning at ∼30s after ICME arrival and lasting until ∼120s after arrival, is the sudden impulse phase. The ground magnetometers exhibit dynamics closely following well-established patterns from observations (Araki, 1977; Araki et al., 1997) and previous MHD simulations (Kataoka et al., 2004; Slinker et al., 1999; Yu & Ridley, 2009b) at all local times. The ΔB_N magnitude reaches $300nT$ at mid latitudes and more than $900nT$ at auroral latitudes. For the northward IMF case, this is the period of the most intense dB_N/dt values (frame b). At low- and mid-latitudes, values agree with the estimates from Tsurutani and Lakhina (2014) ($\sim 30nT/s$). At higher latitudes, extreme dB_N/dt values are observed ($> 200nT/s$). The final phase of the event

is the formation of perturbations related to the the establishment of Dungey-cycle magnetospheric convection as the system reaches a new steady state configuration. Region-1 Birkeland currents form, driving perturbations on the order of several hundred nT. These become static as the system settles, reducing dB_N/dt values to zero.

Frames c-d of Figure 3 illustrate the same but for the case where IMF is southward. Note that the scale of the ΔB_N plot has changed (frame c); the distance between two zero lines (dashed lines) is now 800 nT instead of 300 nT (as in frame a). Again, three phases are evident: the precursor, the sudden impulse signature, and perturbations related to the development of typical region-1 Birkeland currents. Because the polarity of the IMF has changed, the polarity of the precursor signature has flipped. Because the ICME shock is identical to the northward case in terms of dynamic pressure, the sudden impulse signatures are identical, both in terms of polarity, magnitude, and dB/dt. Through the first two phases, the polarity of the IMF plays only a minor role.

The final phase of the commencement stands in stark contrast to the northward case. The southward oriented IMF drives intense reconnection and associated region-1 Birkeland currents. These develop quickly and concurrently with the end of the sudden commencement signature. The superposition of the sudden commencement signal and the intense Birkeland current signal creates perturbations that reach into the thousands of nanotesla with dB/dt values that reach 300 nT/s. The final phase of the event prolongs the GIC threat beyond what is presented by the northward case. The erosion of the day side magnetopause also brings the Birkeland currents to lower latitudes on the day side, bringing the threat over more populated areas of the globe.

The magnitudes of dB/dt are dependent both on latitude and longitude. Figure 4 summarizes the maximum dB_N/dt for -2:00<T-T$_{Arrival}$ <5:00 and local times between dawn and dusk. On the night side, complicated tail dynamics present a complicated picture that will be the focus of future studies and not addressed here. Further, east-west component values remain at or below the north-south values shown in Figure 4.

Figure 4 illustrates the danger presented during the arrival of a perfect, isolated ICME. It is evident that the strongest dB/dt values occur at local noon between 55° and 65° latitude. However, extreme values appear across a large region, frequently in excess of the $30nT/s$ estimates provided by Tsurutani and Lakhina (2014). The red lines in Figure 4 mark the latitude boundary above which $dB/dt > 30nT/s$. For the northward IMF case (frame a), this boundary straddles 50°. For the southward IMF case (frame b), this boundary reaches as low as 40°. It is important to note that because these simulations used a simplified dipole axis, extreme dB/dt could reach lower geographic latitudes in a real world situation, easily encroaching into the continental United States of America.

5 Historical Context

Table 1 places the results of the above simulations in the context of other simulations and real-world observations of extreme sudden commencements. Where available, the impulse as measured by Dst (or equivalent), the magnetopause stand-off distance, and the maximum reported dB/dt are shown. While not an exhaustive list, it emphasizes the most prominent space weather events that should be comparable to the hypothetical ICME in question.

Overall, the hypothetical most-extreme storm sudden commencement simulated here surpasses magnitudes presented by its peers. Estimates from the Tsurutani and Lakhina (2014) (Table 1, top row) are accurate in terms of the strength of the impulse as measured by D$_{ST}$, but underestimate compression/erosion of the day side magnetopause and dB/dt at mid- to high- latitudes. An attempt to produce conditions similar to the famous Carrington Event (fourth row) yields magnetopause compression similar to that

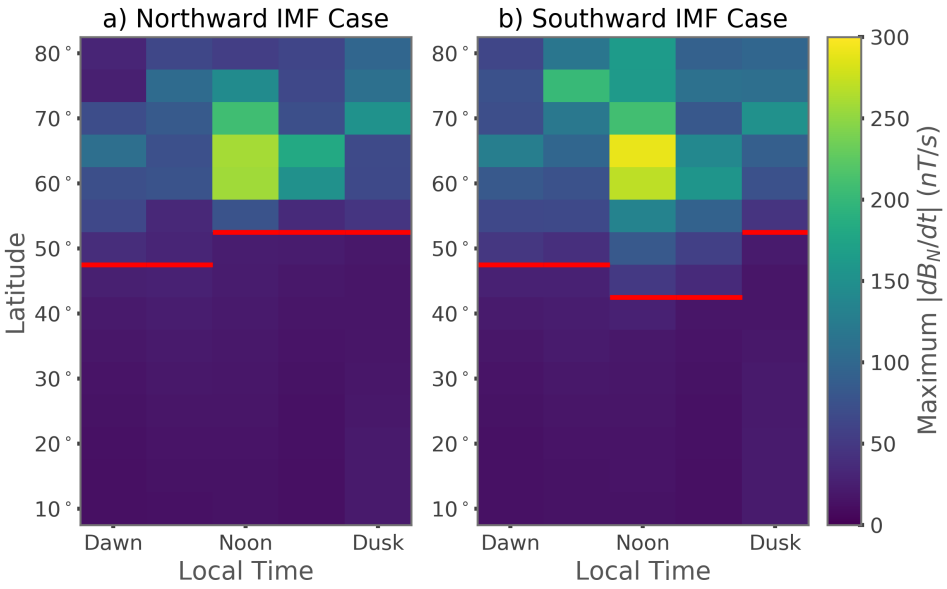

Figure 4. Maximum dB_N/dt from -2:00<T-T$_{Arrival}$ <5:00 as a function of local time (x-axis) and latitude (y-axis). Results for the northward and southward case (frame a and b, respectively) are shown. Red lines mark the contour of $30nT/s$.

Table 1. Comparison of simulation results to other extreme space weather events & simulations.

Event/Simulation	D_{ST} Impulse	Standoff Distance	Maximum dB/dt
T & L Estimates[1]	245 nT	5 R_E	30 nT/s
Present Results: NB_Z	234.0 nT	4 R_E	12 to 260 nT/s
Present Results: SB_Z	268.7 nT	$< 3R_E$	12 to 290 nT/s
Synthetic Carrington[2]	< 200 nT	>2 R_E	N/A
July 2012 near-miss[3,4]	No strong impulse	N/A	~ 10 nT/s
September 1909 Storm[5]	~ 70.0	5.9	N/A
May 1921 Storm[6]	~ 107.0	5.3	N/A
March 1989 Storm[7]	~ 70 nT	N/A	~ 20 nT/s
March 24, 1991 Storm[8,9]	202 nT	N/A	~ 20 nT/s at MSR

[1]Tsurutani and Lakhina (2014), [2]Ngwira et al. (2014), [3]Baker et al. (2013), [4]Ngwira et al. (2013), [5]Love, Hayakawa, and Cliver (2019b), [6]Love, Hayakawa, and Cliver (2019a), [7]Kappenman (2005), [8]Allen, Sauer, Frank, and Reiff (1989), [8]Araki et al. (1997), [9]Araki (2014)

found here, but a weaker sudden commencement D_{ST}. "What If" simulations of the July 2012 near-miss extreme CME (Ngwira et al. (2013); fifth row) show that it would have not produced a significant sudden commencement; peak dB/dt for this hypothetical were much lower than those found in this study. The September 1909, May 1921 "railroad," and the March 1989 "HydroQuebec" historical extreme storms (Table 1, Rows 6-8, respectively) all delivered sudden commencements far weaker than the hypothetical worst-case explored here. The HydroQuebec event of 1989 famously disrupted power distribution in eastern Canada; peak dB/dt values are as much as an order-of-magnitude less than those found in the present simulations. In each of the above cases, the characteristic magnitudes of the simulated worst-case scenario are notably greater.

An interesting outlier is the March 24, 1991 storm (Table 1, bottom row). This event produced an anomalously large sudden commencement as measured on the ground: 202 nT in the H-component of the Kakioka ground station (Araki et al., 1997). While the overall storm is not as famous or destructive as the March 1989 event, large geomagnetically induced currents were reported in the HydroQuebec (Bolduc, 2002) and northern European (Pirjola, 2005) power grids. A handful of other extreme storm sudden commencements with ground amplitudes commensurate with the present hypothetical worst-case simulations have been reported by Araki (2014), suggesting that the results here are not out of the realm of possibility.

6 Discussion & Conclusions

The estimates of the impacts of a "perfect" ICME arrival at Earth, as given by Tsurutani and Lakhina (2014), paints an incomplete picture of the full hazards of such an event. The first-principles-based simulations performed in this study show the full impact at a range of locations. Magnetopause compression exceeds the pressure-balance-based estimates from the previous work. The magnitude and nature of the ground magnetic perturbation is heavily location dependent. This analysis shows that the $30nT/s$ estimates from Tsurutani and Lakhina (2014) are easily surpassed above $\sim 45^{\circ}$ geomagnetic latitude. Accounting for the dipole tilt and time of arrival means that densely-populated lower geographic latitudes can be impacted by the extreme dB/dt values found in these simulations. While the day side is most strongly affected, extreme perturbations are found across the globe. Though only the initial moments of such an event are considered, this sudden impulse would surpass its real world peers in terms of dB/dt.

The orientation of the IMF plays a critical role in determining the severity of the ground response during the impulse. As day side reconnection develops, erosion of the day side field combines with compression to drive the magnetopause within 3 R_E of the Earth. While compression-related magnetic perturbations between the purely northward and purely southward simulation are nearly identical, the development of intense region-1 Birkeland currents in the southward IMF case increase both the magnitude and the duration of the ground perturbations. The erosion of the day side magnetopause pushes these currents and their associated perturbations to far lower latitudes than the northward case. This means that even during the first moments of an extreme space weather storm, IMF orientation plays a critical role in determining the danger to vulnerable technological systems. Further exploring the parameter space of the IMF orientation will help quantify the full range of impacts as a function of impact angle (e.g., Oliveira et al., 2018; Oliveira & Raeder, 2014, 2015).

Many limitations must be considered when interpreting these results, starting with the construction of the idealized solar wind and IMF conditions. The work of Tsurutani and Lakhina (2014) merely provides amplitudes. Here, these amplitudes have been adapted into a simple step function. In reality, a more complicated sheath region would form, with strong oscillations in IMF and plasma conditions. The transition to fully southward or northward IMF are not likely to be simultaneous with the pressure increase. Further, the plasma density used here, $20cm^{-3}$, is frequently surpassed in real-world ICMEs. This could be considered a lower bound for a real world event. While considering these factors should be a priority in the future, the results of this study still provide meaningful estimates of an extreme impulse.

Further work is required to fully tie ICME arrival to consequences for the power grid. dB/dt, while clearly tied to geomagnetically induced currents (GICs), is not the value of interest. Geoelectric field must be calculated by including the ground impedance. This means accounting for the effects of an inhomogeneous conducting crust, lithosphere, and ocean. Higher frequency components of the impulse can be reflected by the conducting Earth, intensifying the surface response. It is also important to note that it is not

just the geoelectric field amplitude, but also spectral content that affects the power grid. These must be further examined to understand the precise impact such an event would have on power transmission.

Despite these shortcomings, this work stands as an important indicator of the activity possible during the first moments after arrival of a "perfect" ICME at Earth. The magnitude of dB/dt, compression and erosion of the day side magnetopause, and short time scales for the onset of activity make such an event uniquely threatening to ground-based infrastructure. The penetration of activity to mid-latitudes early in the event will affect regions not prepared for such strong geomagnetic activity, raising the vulnerability of power grids in populated areas. Further exploring and preparing for such extreme activity is important to mitigate space-weather related catastrophes.

Acknowledgments

The authors would like to thank Dr. Michael Wiltberger for providing his expertise to this project. We thank A. Kelbert and K. Lewis for reading a draft manuscript. This work was funded by the Laboratory Directed Research and Development (LDRD) program grant 20170047DR and the National Science Foundation award ICER-1663770. Model result data and input files are available via https://doi.org/10.5281/zenodo.3620786. The Space Weather Modeling Framework is maintained by the University of Michigan Center for Space Environment Modeling and can be obtained at http://csem.engin.umich.edu/tools/swmf. We would like to acknowledge high-performance computing support from Cheyenne (doi:10.5065/D6RX99HX, allocation UUSL0016) provided by NCAR's Computational and Information Systems Laboratory, sponsored by the National Science Foundation.

References

Allen, J., Sauer, H., Frank, L., & Reiff, P. (1989). Effects of the March 1989 solar activity. *Eos, Transactions American Geophysical Union*, *70*(46), 1479. Retrieved from http://doi.wiley.com/10.1029/89EO00409 doi: 10.1029/89EO00409

Araki, T. (1977). Global structure of geomagnetic sudden commencements. *Planetary and Space Science*, *25*(4), 373–384. doi: 10.1016/0032-0633(77)90053-8

Araki, T. (2014). Historically largest geomagnetic sudden commencement (SC) since 1868. *Earth, Planets and Space*, *66*, 1–6. Retrieved from http://www.earth-planets-space.com/content/66/1/164 doi: 10.1186/s40623-014-0164-0

Araki, T., Fujitani, S., Emoto, M., Yumoto, K., Shiokawa, K., Ichinose, T., ... Liu, C. F. (1997). Anomalous sudden commencement on March 24, 1991. *Journal of Geophysical Research*, *102*(A), 14075–14086. Retrieved from http://adsabs.harvard.edu/cgi-bin/nph-data{_}query?bibcode=1997JGR...10214075A{\&}link{_}type=ABSTRACT{\%}5Cnpapers3://publication/doi/10.1029/96JA03637 doi: 10.1029/96JA03637

Baker, D. N., Li, X., Pulkkinen, A., Ngwira, C. M., Mays, M. L., Galvin, A. B., & Simunac, K. D. C. (2013, oct). A major solar eruptive event in July 2012: Defining extreme space weather scenarios. *Space Weather*, *11*(10), 585–591. Retrieved from http://doi.wiley.com/10.1002/swe.20097 doi: 10.1002/swe.20097

Bolduc, L. (2002, nov). GIC observations and studies in the Hydro-Québec power system. *Journal of Atmospheric and Solar-Terrestrial Physics*, *64*(16), 1793–1802. Retrieved from https://www.sciencedirect.com/science/article/pii/S1364682602001281 doi: 10.1016/S1364-6826(02)00128-1

Cannon, P., Angling, M., Barclay, L., Curry, C., Dyer, C., Edwards, R., ... Underwood, C. (2013). *Extreme space weather:impacts on engineered systems and infrastructure*. Royal Academy of Engineering.

De Zeeuw, D., Gombosi, T., Groth, C., Powell, K., & Stout, Q. (2000). An

adaptive MHD method for global space weather simulations. *IEEE Transactions on Plasma Science*, *28*(6), 1956–1965. Retrieved from http://ieeexplore.ieee.org/lpdocs/epic03/wrapper.htm?arnumber=902224 doi: 10.1109/27.902224

De Zeeuw, D. L., Sazykin, S., Wolf, R. A., Gombosi, T. I., Ridley, A. J., & Tóth, G. (2004). Coupling of a global MHD code and an inner magnetospheric model: Initial results. *Journal of Geophysical Research: Space Physics*, *109*(A12), A12219. Retrieved from http://doi.wiley.com/10.1029/2003JA010366 doi: 10.1029/2003JA010366

Eastwood, J. P., Biffis, E., Hapgood, M. A., Green, L., Bisi, M. M., Bentley, R. D., ... Burnett, C. (2017, feb). The Economic Impact of Space Weather: Where Do We Stand? *Risk Analysis*, *37*(2), 206–218. Retrieved from http://doi.wiley.com/10.1111/risa.12765 doi: 10.1111/risa.12765

Glocer, A. (2016, oct). Coupling Ionospheric Outflow into Magnetospheric Models. In *Agu monograph series* (pp. 195–203). Hoboken, NJ, USA: John Wiley & Sons, Inc. Retrieved from http://doi.wiley.com/10.1002/9781119066880.ch15 doi: 10.1002/9781119066880.ch15

Gonzalez, W. D., de Gonzalez, A. L. C., Dal Lago, A., Tsurutani, B. T., Arballo, J. K., Lakhina, G. K., ... Wu, S.-T. (1998, apr). Magnetic cloud field intensities and solar wind velocities. *Geophysical Research Letters*, *25*(7), 963–966. Retrieved from http://doi.wiley.com/10.1029/98GL00703 doi: 10.1029/98GL00703

Gonzalez, W. D., Echer, E., Tsurutani, B. T., De Gonzalez, A. L., & Dal Lago, A. (2011, jan). Interplanetary origin of intense, superintense and extreme geomagnetic storms. In *Space science reviews* (Vol. 158, pp. 69–89). Springer Netherlands. Retrieved from http://link.springer.com/10.1007/s11214-010-9715-2 doi: 10.1007/s11214-010-9715-2

Groth, C. P. T., De Zeeuw, D. L., Gombosi, T. I., & Powell, K. G. (2000). Global three-dimensional MHD simulation of a space weather event: CME formation, interplanetary propagation, and interaction with the magnetosphere. *Journal of Geophysical Research*, *105*(A11), 25053. Retrieved from http://doi.wiley.com/10.1029/2000JA900093 doi: 10.1029/2000JA900093

Guo, X. C., Hu, Y. Q., & Wang, C. (2005, dec). Earth's magnetosphere impinged by interplanetary shocks of different orientations. *Chinese Physics Letters*, *22*(12), 3221–3224. doi: 10.1088/0256-307X/22/12/067

Haiducek, J. D., Welling, D. T., Ganushkina, N. Y., Morley, S. K., & Ozturk, D. S. (2017, dec). SWMF Global Magnetosphere Simulations of January 2005: Geomagnetic Indices and Cross-Polar Cap Potential. *Space Weather*, *15*(12), 1567–1587. Retrieved from http://doi.wiley.com/10.1002/2017SW001695 doi: 10.1002/2017SW001695

Harel, M., Wolf, R. A., Reiff, P. H., Spiro, R. W., Burke, W. J., Rich, F. J., & Smiddy, M. (1981). Quantitative simulation of a magnetospheric substorm 1. Model logic and overview. *Journal of Geophysical Research*, *86*(A4), 2217. Retrieved from http://adsabs.harvard.edu/abs/1981JGR....86.2217H doi: 10.1029/JA086iA04p02217

Ilie, R., Liemohn, M. W., & Ridley, A. (2010, jan). The effect of smoothed solar wind inputs on global modeling results. *Journal of Geophysical Research*, *115*(A1), A01213. Retrieved from http://doi.wiley.com/10.1029/2009JA014443 doi: 10.1029/2009JA014443

Joselyn, J. A., & Tsurutani, B. T. (1990, nov). Geomagnetic Sudden impulses and storm sudden commencements: A note on terminology. *Eos, Transactions American Geophysical Union*, *71*(47), 1808–1809. Retrieved from http://doi.wiley.com/10.1029/90EO00350 doi: 10.1029/90EO00350

Kappenman, J. G. (2005). An overview of the impulsive geomagnetic field disturbances and power grid impacts associated with the violent Sun-Earth con-

nection events of 29–31 October 2003 and a comparative evaluation with other contemporary storms. *Space Weather*, *3*(8), S08C01. Retrieved from http://www.agu.org/pubs/crossref/2005/2004SW000128.shtml doi: 10.1029/2004SW000128

Kataoka, R., Fukunishi, H., Fujita, S., Tanaka, T., & Itonaga, M. (2004, mar). Transient response of the Earth's magnetosphere to a localized density pulse in the solar wind: Simulation of traveling convection vortices. *Journal of Geophysical Research: Space Physics*, *109*(A3), A03204. Retrieved from http://doi.wiley.com/10.1029/2003JA010287 doi: 10.1029/2003JA010287

Korth, H., Rastätter, L., Anderson, B. J., & Ridley, A. J. (2011, oct). Comparison of the observed dependence of large-scale Birkeland currents on solar wind parameters with that obtained from global simulations. *Annales Geophysicae*, *29*(10), 1809–1826. Retrieved from http://www.ann-geophys.net/29/1809/2011/angeo-29-1809-2011.htmlhttp://www.ann-geophys.net/29/1809/2011/ doi: 10.5194/angeo-29-1809-2011

Lakhina, G. S., Alex, S., Tsurutani, B. T., & Gonzalez, W. D. (2012). Supermagnetic storms: Hazard to society. *Geophysical Monograph Series*, *196*, 267–278. Retrieved from http://www.agu.org/books/gm/v196/2011GM001073/2011GM001073.shtml doi: 10.1029/2011GM001073

Li, X., Temerin, M., Tsurutani, B., & Alex, S. (2006, jan). Modeling of 1–2 September 1859 super magnetic storm. *Advances in Space Research*, *38*(2), 273–279. Retrieved from http://linkinghub.elsevier.com/retrieve/pii/S0273117705008471 doi: 10.1016/j.asr.2005.06.070

Love, J. J., Hayakawa, H., & Cliver, E. W. (2019a, aug). Intensity and Impact of the New York Railroad Superstorm of May 1921. *Space Weather*, *17*(8), 1281–1292. Retrieved from https://onlinelibrary.wiley.com/doi/abs/10.1029/2019SW002250 doi: 10.1029/2019sw002250

Love, J. J., Hayakawa, H., & Cliver, E. W. (2019b, jan). On the Intensity of the Magnetic Superstorm of September 1909. *Space Weather*, *17*(1), 37–45. Retrieved from https://onlinelibrary.wiley.com/doi/abs/10.1029/2018SW002079 doi: 10.1029/2018SW002079

Manchester, W., Ridley, A., Gombosi, T., & DeZeeuw, D. (2006, jan). Modeling the Sun-to-Earth propagation of a very fast CME. *Advances in Space Research*, *38*(2), 253–262. Retrieved from http://linkinghub.elsevier.com/retrieve/pii/S027311770501210X doi: 10.1016/j.asr.2005.09.044

National Research Committee on the Societal and Economic Impacts of Severe Space Weather Events. (2008, dec). *Workshop Report* (Tech. Rep.). Washington, D.C.. Retrieved from http://www.nap.edu/catalog/12507http://books.google.com/books?hl=en{\&}lr={\&}id={_}nadAgAAQBAJ{\&}oi=fnd{\&}pg=PR1{\&}dq=Severe+Space+Weather+Events--Understanding+Societal+and+Economic+Impacts+Workshop+Report{\&}ots=528WWnRgHQ{\&}sig=jcmLvI75V9hyw-n-1phX50BX--M{\%}5Cnhttp://books doi: 10.17226/12507

National Science and Technology Council. (2015). *National Space Weather Action Plan* (Tech. Rep.). Retrieved from https://www.whitehouse.gov/sites/default/files/microsites/ostp/final{_}nationalspaceweatheractionplan{_}20151028.pdf

Ngwira, C. M., Pulkkinen, A., Kuznetsova, M. M., & Glocer, A. (2014, jun). Modeling extreme "Carrington-type" space weather events using three-dimensional global MHD simulations. *Journal of Geophysical Research: Space Physics*, *119*(6), 4456–4474. Retrieved from http://doi.wiley.com/10.1002/2013JA019661 doi: 10.1002/2013JA019661

Ngwira, C. M., Pulkkinen, A., Leila Mays, M., Kuznetsova, M. M., Galvin, A. B., Simunac, K., ... Glocer, A. (2013, dec). Simulation of the 23 July 2012 extreme space weather event: What if this extremely rare CME was Earth

directed? *Space Weather*, *11*(12), 671–679. Retrieved from http://doi.wiley.com/10.1002/2013SW000990 doi: 10.1002/2013SW000990

Oliveira, D. M., Arel, D., Raeder, J., Zesta, E., Ngwira, C. M., Carter, B. A., ... Gjerloev, J. W. (2018, jun). Geomagnetically Induced Currents Caused by Interplanetary Shocks With Different Impact Angles and Speeds. *Space Weather*, *16*(6), 636–647. Retrieved from http://doi.wiley.com/10.1029/2018SW001880 doi: 10.1029/2018SW001880

Oliveira, D. M., & Raeder, J. (2014). Impact angle control of interplanetary shock geoeffectiveness. *Journal of Geophysical Research: Space Physics*, *119*(10), 8188–8201. doi: 10.1002/2014JA020275

Oliveira, D. M., & Raeder, J. (2015, jun). Impact angle control of interplanetary shock geoeffectiveness: A statistical study. *Journal of Geophysical Research: Space Physics*, *120*(6), 4313–4323. Retrieved from https://onlinelibrary.wiley.com/doi/abs/10.1002/2015JA021147 doi: 10.1002/2015JA021147

Pirjola, R. (2005, jan). Effects of space weather on high-latitude ground systems. *Advances in Space Research*, *36*(12), 2231–2240. Retrieved from https://www.sciencedirect.com/science/article/pii/S0273117705000025{\#}bib1 doi: 10.1016/j.asr.2003.04.074

Powell, K., Roe, P., & Linde, T. (1999, sep). A solution-adaptive upwind scheme for ideal magnetohydrodynamics. *Journal of Computational Physics*, *154*(2), 284–309. Retrieved from http://linkinghub.elsevier.com/retrieve/pii/S002199919996299Xhttp://www.sciencedirect.com/science/article/pii/S002199919996299X doi: 10.1006/jcph.1999.6299

Pulkkinen, A., Rastätter, L., Kuznetsova, M., Singer, H., Balch, C., Weimer, D., ... Weigel, R. (2013, jun). Community-wide validation of geospace model ground magnetic field perturbation predictions to support model transition to operations. *Space Weather*, *11*(6), 369–385. Retrieved from http://doi.wiley.com/10.1002/swe.20056 doi: 10.1002/swe.20056

Rastätter, L., Kuznetsova, M. M., Glocer, A., Welling, D., Meng, X., Raeder, J., ... Gannon, J. (2013, apr). Geospace environment modeling 2008-2009 challenge: D st index. *Space Weather*, *11*(4), 187–205. Retrieved from http://doi.wiley.com/10.1002/swe.20036 doi: 10.1002/swe.20036

Rastätter, L., Kuznetsova, M. M., Vapirev, A., Ridley, A., Wiltberger, M., Pulkkinen, A., ... Singer, H. J. (2011, apr). Geospace Environment Modeling 2008–2009 Challenge: Geosynchronous magnetic field. *Space Weather*, *9*(4), S04005. Retrieved from http://onlinelibrary.wiley.com/doi/10.1029/2010SW000617/full doi: 10.1029/2010SW000617

Ridley, A., De Zeeuw, D., Manchester, W., & Hansen, K. (2006, jan). The magnetospheric and ionospheric response to a very strong interplanetary shock and coronal mass ejection. *Advances in Space Research*, *38*(2), 263–272. Retrieved from http://linkinghub.elsevier.com/retrieve/pii/S0273117706003966 doi: 10.1016/j.asr.2006.06.010

Ridley, A. J., De Zeeuw, D. L., Gombosi, T. I., & Powell, K. G. (2001). Using steady state MHD results to predict the global state of the magnetosphere-ionosphere system. *Journal of Geophysical Research*, *106*(A12), 30067. Retrieved from http://doi.wiley.com/10.1029/2000JA002233 doi: 10.1029/2000JA002233

Ridley, A. J., Hansen, K. C., Toth, G., DeZeeuw, D. L., Gombosi, T., & Powell, K. G. (2002). University of Michigan MHD results of the Geospace Global Circulation Model metrics challenge. *Journal of Geophysical Research*, *107*(A10), 1290. Retrieved from http://doi.wiley.com/10.1029/2001JA000253 doi: 10.1029/2001JA000253

Sazykin, S., & Stanislav. (2000). Theoretical studies of penetration of magnetospheric electric fields to the ionosphere. *Thesis (PhD). UTAH STATE*

UNIVERSITY, Source DAI-B 61/12, p. 6521, Jun 2001, 278 pages..

Schrijver, C. J. (2015). Socio-economic hazards and impacts of space weather: the important range between mild and extreme. *Space Weather*, n/a–n/a. Retrieved from http://doi.wiley.com/10.1002/2015SW001252 doi: 10.1002/2015SW001252

Slinker, S. P., Fedder, J. A., Emery, B. A., Baker, K. B., Lummerzheim, D., Lyon, J. G., & Rich, F. J. (1999, dec). Comparison of global MHD simulations with AMIE simulations for the events of May 19-20, 1996. *Journal of Geophysical Research: Space Physics*, *104*(A12), 28379–28395. Retrieved from http://doi.wiley.com/10.1029/1999JA900403 doi: 10.1029/1999JA900403

Song, P., DeZeeuw, D. L., Gombosi, T. I., Groth, C. P. T., & Powell, K. G. (1999). A numerical study of solar wind—magnetosphere interaction for northward interplanetary magnetic field. *Journal of Geophysical Research*, *104*(A12), 28361. Retrieved from http://adsabs.harvard.edu/abs/1999JGR...10428361S doi: 10.1029/1999JA900378

Toffoletto, F., Sazykin, S., Spiro, R., & Wolf, R. (2003). Inner magnetospheric modeling with the Rice Convection Model. *Space Science Reviews*(1), 175–196. Retrieved from http://adsabs.harvard.edu/abs/2003SSRv..107..175T doi: 10.1023/A:1025532008047

Tóth, G., Sokolov, I. V., Gombosi, T. I., Chesney, D. R., Clauer, C. R., De Zeeuw, D. L., ... Kóta, J. (2005). Space Weather Modeling Framework: A new tool for the space science community. *Journal of Geophysical Research*, *110*(A12), A12226. Retrieved from http://www.agu.org/pubs/crossref/2005/2005JA011126.shtml doi: 10.1029/2005JA011126

Tóth, G., van der Holst, B., Sokolov, I. V., De Zeeuw, D. L., Gombosi, T. I., Fang, F., ... Opher, M. (2012, feb). Adaptive numerical algorithms in space weather modeling. *Journal of Computational Physics*, *231*(3), 870–903. Retrieved from http://www.sciencedirect.com/science/article/pii/S002199911100088X doi: 10.1016/j.jcp.2011.02.006

Tsurutani, B. T. (2003). The extreme magnetic storm of 1–2 September 1859. *Journal of Geophysical Research*, *108*(A7), 1268. Retrieved from http://doi.wiley.com/10.1029/2002JA009504 doi: 10.1029/2002JA009504

Tsurutani, B. T., & Lakhina, G. S. (2014, jan). An extreme coronal mass ejection and consequences for the magnetosphere and Earth. *Geophysical Research Letters*, *41*(2), 287–292. Retrieved from http://doi.wiley.com/10.1002/2013GL058825 doi: 10.1002/2013GL058825

Wang, C., Li, C. X., Huang, Z. H., & Richardson, J. D. (2006, jul). *Effect of interplanetary shock strengths and orientations on storm sudden commencement rise times* (Vol. 33) (No. 14). doi: 10.1029/2006GL025966

Welling, D. (2019, sep). Magnetohydrodynamic Models of B and Their Use in GIC Estimates. In J. L. Gannon, A. Swidinsky, & Z. Xu. (Eds.), *Geomagnetically induced currents from the sun to the power grid (in press)* (Geophysica ed., pp. 43–65). American Geophysical Union (AGU). Retrieved from https://onlinelibrary.wiley.com/doi/abs/10.1002/9781119434412.ch3 doi: 10.1002/9781119434412.ch3

Welling, D. T., Jordanova, V. K., Glocer, A., Toth, G., Liemohn, M. W., & Weimer, D. R. (2015, jun). The two-way relationship between ionospheric outflow and the ring current. *Journal of Geophysical Research: Space Physics*, *120*(6), 4338–4353. Retrieved from http://doi.wiley.com/10.1002/2015JA021231 doi: 10.1002/2015JA021231

Welling, D. T., & Ridley, A. J. (2010, apr). Exploring sources of magnetospheric plasma using multispecies MHD. *Journal of Geophysical Research*, *115*(A4), A04201. Retrieved from http://doi.wiley.com/10.1029/2009JA014596 doi: 10.1029/2009JA014596

Welling, D. T., & Zaharia, S. G. (2012, dec). Ionospheric outflow and cross polar

cap potential: What is the role of magnetospheric inflation? *Geophysical Research Letters*, *39*(23), n/a–n/a. Retrieved from http://doi.wiley.com/10.1029/2012GL054228 doi: 10.1029/2012GL054228

Yu, Y., & Ridley, A. J. (2008, may). Validation of the space weather modeling framework using ground-based magnetometers. *Space Weather*, *6*(5), S05002. Retrieved from http://www.agu.org/pubs/crossref/2008/2007SW000345.shtml doi: 10.1029/2007SW000345

Yu, Y., & Ridley, A. J. (2009a, dec). The response of the magnetosphere-ionosphere system to a sudden dynamic pressure enhancement under southward IMF conditions. *Annales Geophysicae*, *27*(12), 4391–4407. Retrieved from http://www.ann-geophys.net/27/4391/2009/ doi: 10.5194/angeo-27-4391-2009

Yu, Y., & Ridley, A. J. (2009b, mar). Response of the magnetosphere-ionosphere system to a sudden southward turning of interplanetary magnetic field. *Journal of Geophysical Research*, *114*(A3), A03216. Retrieved from http://doi.wiley.com/10.1029/2008JA013292 doi: 10.1029/2008JA013292

Zhang, J., Liemohn, M. W., De Zeeuw, D. L., Borovsky, J. E., Ridley, A. J., Toth, G., ... Wolf, R. A. (2007, apr). Understanding storm-time ring current development through data-model comparisons of a moderate storm. *Journal of Geophysical Research*, *112*(A4), A04208. Retrieved from http://doi.wiley.com/10.1029/2006JA011846 doi: 10.1029/2006JA011846